Lipid Demixing Reduces Energy Barriers for High Curvature Vesicle Budding

Itay Schachter*
Institute of Organic Chemistry and Biochemistry of the Czech Academy of Sciences, Flemingovo nám. 542/2, CZ-16000 Prague 6, Czech Republic and Institute of Chemistry, the Fritz Haber Research Center, and the Harvey M. Kruger Center for Nanoscience & Nanotechnology, The Hebrew University, Jerusalem 9190401, Israel
(Dated: October 24, 2024)

Under standard physiological conditions, budding relies on asymmetries, including differences in leaflet composition, area, and osmotic conditions, and involves large curvature changes in nanoscale lipid vesicles. So far, the combined impact of asymmetry and high curvatures on budding has remained unknown. Here, using continuum elastic theory, the budding pathway is detailed under realistic conditions. The model enables a quantitative description of the budding process and the budded state of both ideally and non-ideally mixed lipid nanoscale vesicles. It shows that budding is less favored in smaller vesicles but lipid demixing can significantly reduce its energy barrier and yet high compositional deviations of more than 7% between the bud and vesicle only occur with phase separation on the bud.

Nanoscale budding plays a crucial role in key biological processes such as endocytosis, viral budding [1] and intraluminal vesicle formation [2]. Budding is defined as a process wherein a single closed membrane undergoes a sequence of shape changes, ultimately leading to the formation of a distinct daughter vesicle (DV) connected to the original membrane via a narrow neck (Fig. 1A). Here, the closed membrane is set as a spherical or prolate mother vesicle (MV). Budding may become energetically favorable whenever some asymmetry arises between the outer and inner leaflets (Fig. 1B), such as in lipid or solution composition, area, osmotic conditions or a combination of these [3]. These asymmetries are prevalent in cells and organelles [4–7], with transmembrane proteins such as lipid transporters and channels, modulating the membrane asymmetry and influence highly-regulated biological processes involving budding [8, 9]. Thus, understanding the impact of asymmetry on budding may enhance our comprehension of the regulation of processes—such as viral budding, their pathologies and their sensitivity to asymmetry in general. The area-difference elasticity (ADE) model [10] specifically predicts that a combination of area asymmetry, lower than ideal vesicle water content and a positive bilayer spontaneous curvature—due to lipid or solution composition asymmetry—may induce outward budding. However, the combined contribution of the possible asymmetries to budding, especially at the nanoscale, has thus far remained enigmatic.

For experiments, layer-by-layer assembly and outer-leaflet modification methods [11, 12], such as lipid exchange and enzymatic modification, enable the creation of asymmetrical model vesicles in terms of composition and possibly leaflet area. These methods allow the study of how asymmetry affects membrane properties and processes [13–17]. However, significant variations between vesicles within a sample limit the experimental accuracy.

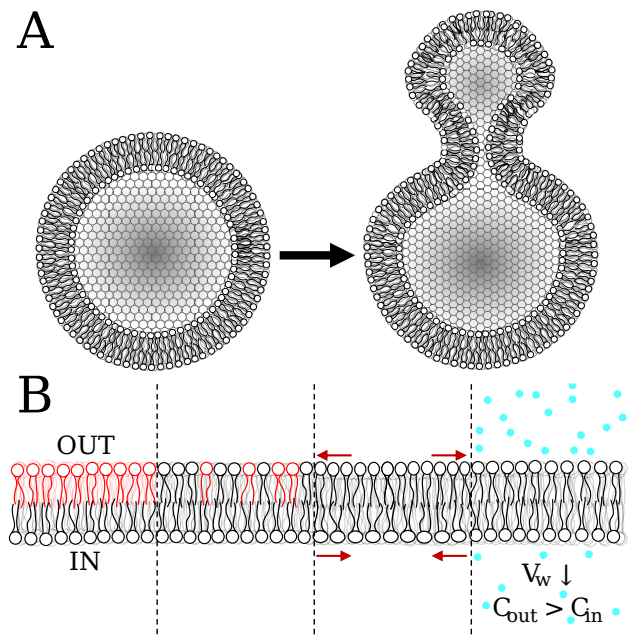

FIG. 1. (A) Illustration, not to scale, of the initial (left) and final (right) states of outward budding. Initially, no significant curvature is present. In the final, budded state, high curvature appears at the neck region and the DV. (B) Types of membrane asymmetries: 1. Composition: Completely asymmetric (left) or partially asymmetric (middle left), as seen in vesicles from layer-by-layer assembly and some outer-leaflet modification methods, respectively. 2. Leaflet area: Non-ideal lipid numbers in each leaflet cause opposite stresses (middle right). 3. Osmotic conditions: Hypotonic conditions reduce the volume of entrapped water (right).

These variations are in the degree of composition asymmetry [11], vesicle size [18], and water content [19]. Also, imaging nanoscale budding requires techniques such as electron microscopy, which lack the temporal resolution to fully capture this dynamic process [20]. While molec-

* itay.schachter@mail.huji.ac.il

ular dynamics (MD) simulations offer the necessary spatial and temporal resolutions and allow for high control over parameters like the degree of asymmetry, they are currently restricted by their limited scales [21]. Even with these limitations overcome, relying solely on experiments and simulations without theoretical frameworks is insufficient for comprehending the forces driving budding. Thus, a theoretical description is required to fully understand this process.

In nanoscale vesicles, budding generates relatively high curvatures at the nanometer-sized DV as well as the neck region. The ADE model struggles in this scenario because it relies on the assumption that the membrane thickness is negligible compared to the vesicle radius. The impact of a non-negligible membrane thickness on budding, to the best of the author's knowledge, has not been previously quantified in the literature. Furthermore, as was suggested in a recent experimental study [17], the high curvature differences may induce local lipid sorting, yielding substantially different compositions between the MV, DV, and the neck region. An extension of the ADE model addresses membrane heterogeneity [22], though it still faces the same key limitations as the original model.

Here, I use a highly-detailed elastic model to investigate the budding process, which circumvents the limitations of previous experimental and theoretical studies. It describes a single nanoscale vesicle under relevant experimental and physiological conditions. The findings reveal that budding is more prohibited in these vesicles. Also, lipid heterogeneity, similar to that in cells and organelles, can lower the budding energy barrier, though significant lipid sorting requires domain formation.

Building on the formalism that extends the Helfrich–Hamm–Kozlov model [23–25], as detailed by Ryham et al. [26–28], this study presents a continuum model for an enclosed vesicle (Fig. 2A); Section S1 details the implementation. For each leaflet ($j = o, i$, denoting outer and inner), the lipid vector field $\boldsymbol{D}_j = l_j \boldsymbol{n}_j$ describes the local (relaxed) lipid length l_j (l_0) and the unit lipid director normal $\boldsymbol{n}_j$. This field, defined over the leaflet neutral surface S_j, points from the neutral surface to the midplane surface S_m. Cylindrical symmetry is assumed for these surfaces. The elastic contribution to the free energy for each leaflet, based on the modes of deformation shown in Fig. 2B, is given by

$$F_j^{\mathrm{el}} = \frac{1}{2}\int_{S_j} \{K_C[(2H+J_s)^2 - J_s^2] + \kappa_t \boldsymbol{t}^2 + K_a \alpha^2\} \mathrm{d}S_j \quad (1)$$

The first term represents the bending energy, with the bending modulus K_C determining the energy penalty for splay deformations, $2H = \nabla \cdot \boldsymbol{n}$, from its natural value, defined as minus the spontaneous curvature J_s (positive for a spherical micelle). The second term describes the tilt energy governed by the tilt modulus κ_t and the tilt deformation $\boldsymbol{t} = \boldsymbol{n}/(\boldsymbol{N}\cdot\boldsymbol{n}) - \boldsymbol{N}$, where $\boldsymbol{N}$ is the surface normal. The final term defines the area-compressibility energy with modulus K_a for deviations in the local area-

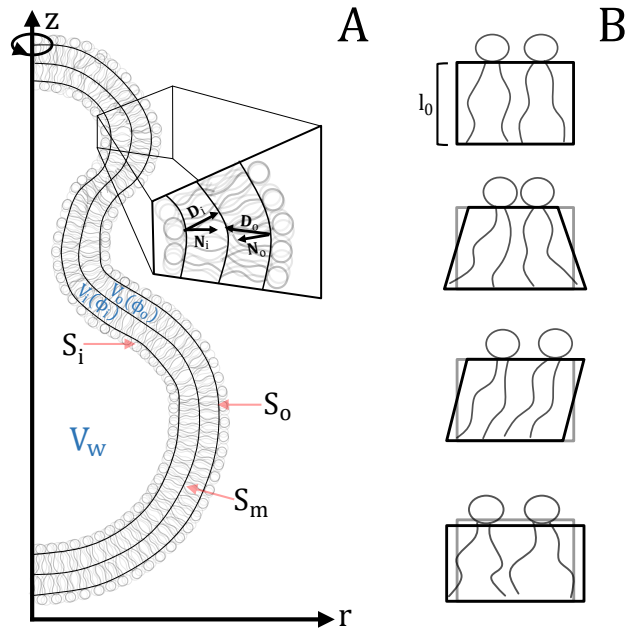

FIG. 2. (A) Schematic view of a budded vesicle showing the vector fields described in the main text. (B) Schematic of the modes of deformation considered by the elastic theory, from top to bottom: undeformed, bend, tilt and area stretch.

per-lipid (APL), a, from its relaxed value, a_0, described by $\alpha = \frac{a-a_0}{\sqrt{a_0 a}}$. Assuming local lipid incompressibility ($al = a_0 l_0$), $\alpha = \frac{l_0 - l}{\sqrt{l_0 l}}$.

The model includes volume constraints to accurately describe the physical and experimental conditions. Each leaflet's volume is kept constant, reflecting global lipid incompressibility and the negligible rate of phospholipid flip-flop [29]. The volume of the entrapped water is also set constant, as it remains practically unchanged under specific osmotic conditions [3] and is influenced by them and by the vesicle fabrication method [19]. The model was validated under various scenarios (Section S1 A) and is available on GitHub.

Consider an initially spherical vesicle with a midplane radius, $R_m = 50$ nm. The difference in the (relaxed) area between the outer and inner leaflets is $\Delta A = 4 l_0 R_m m_0$, where m_0 is a unitless factor accounting for leaflet area asymmetry. For no asymmetry, $m_0 = 4\pi$; m_0 is larger (smaller) than 4π when the outer leaflet has a lipid excess (deficiency) and vice versa for the inner leaflet. The entrapped water volume, V_w, may deviate from its ideal value of $V_w^{\mathrm{id}} = 4\pi(R_m - l_0)^3/3$, such that $V_w = \nu V_w^{\mathrm{id}}$, with ν defined as the relative water content factor. Using these two factors, m_0 and ν, the equilibrium phase was determined, yielding a phase diagram (Fig. 3).

The non-negligible monolayer thickness relative to the vesicle radius ($l_0 \not\ll R_m$) makes budding less favorable because the coexistence curve in the (ν, m_0) plane shifts upwards when a typical l_0 of 1.5 nm is chosen. This

shift is particularly pronounced for vesicles with nearly ideal water content volume ($\nu \approx 1$), making budding more inhibited in them. When $l_0 \ll R_m$, the bending free energy density is described as a function of the mid-plane mean curvature, H, via $K_C(2H)^2$. For nanoscale vesicles, however, positive higher-order terms, linear in l_0 [30], contribute enough to the bending free energy to somewhat inhibit budding.

The coexistence curve for the thinner membrane ($l_0 = 0.5$ nm) closely aligns with the one predicted by the ADE model. A comparison of the current model results with those provided in the original paper of the ADE model [10] reveals a minor but consistent miscalculation in that paper, further detailed in Section S2. Nevertheless, the ADE model provides a good approximation when $l_0/R_m \approx 0.01$ or lower, i.e., for vesicles with a radius of several hundred nanometers.

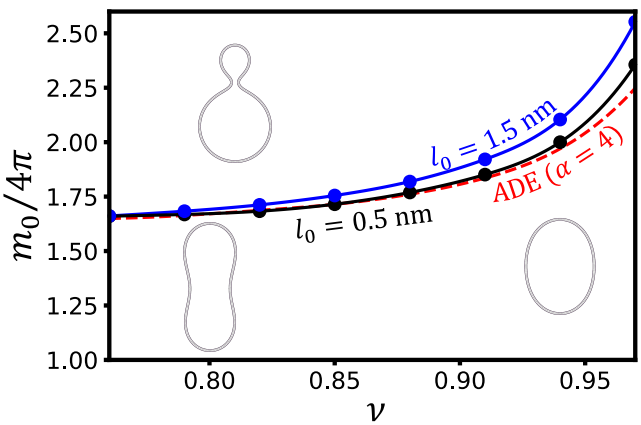

FIG. 3. Phase diagram of the elastic model in the (ν, m_0) plane involving budding. The coexistence curve between the prolate and budded states, interpolated with a cubic spline (solid lines) between sampled values (circles), shifts upward with monolayer thickness, l_0. Other elastic parameters are $K_C = 10\ k_\mathrm{B}T$, $\kappa_t = 10\ k_\mathrm{B}T\ \mathrm{nm}^{-2}$, and $K_a = \alpha\pi K_C l_0^{-2}$ with $\alpha = 4$. As $l_0 \to 0$, the curve should nearly coincide with the ADE model's prediction from Ref. 10 for $\alpha = 4$ (dashed red line); the curve shown was originally suggested for $\alpha = 1$ (see Section S2).

Here, the model is extended to include lateral compositional variation. For simplicity, we will focus on binary lipid mixtures. To this aim, a scalar field ϕ, representing the molar ratio of the additional lipid, is defined over S_j. Consequently, the model now includes a mixing free energy contribution in mixed leaflets, relative to homogeneous mixing with $\phi_0 = \langle\phi\rangle$. This contribution is expressed as $F_j^{\mathrm{mix}} = \int_{S_j} f^{\mathrm{mix}}(\phi)\,\mathrm{d}S_j$, where $f^{\mathrm{mix}}(\phi)$ is the mixing free energy density. Specifically, f^{mix} is chosen as

$$\frac{f^{\mathrm{mix}}(\phi)\cdot a}{k_\mathrm{B}T} = \phi\log\left(\frac{\phi}{\phi_0}\right) + (1-\phi)\log\left(\frac{1-\phi}{1-\phi_0}\right) + \chi\phi\,(\phi_0-\phi) + K|\nabla\phi|^2 \qquad (2)$$

The first two terms describe the ideal mixing entropy between the components, while the third term introduces a non-ideal interaction between the two lipids, whose magnitude is dictated by an interaction parameter, χ. The last term details the penalty for spatial variations in the composition and ensures that ϕ remains continuous; further details in Section S1. In a planar membrane, phase separation can occur when $\chi > 2$, because f^{mix} then has two points of common tangent. Analysis of MD simulations shows that eq 2 effectively captures the extent of mixing for different binary mixtures over a wide range of ϕ values (Section S4). Similarly to the volume constraints, the average composition of mixed leaflets is maintained. Elastic deformations promote demixing whenever lipids have different physical properties [31–33]. The model only includes variations in J_s, which is intimately related to lipid geometry [34], as the membrane shape is very sensitive to it [35]. It varies linearly between its values for the two components with the local composition; i.e., $J_s(\phi) = J_s(1-\phi) + \tilde{J}_s\phi$, where $\tilde{J}_s$ is its value for the additional lipid.

The default lipid parameters in the model for the subsequent analyses match those of 1-palmitoyl-2-oleoyl-*sn*-glycero-3-phosphocholine (POPC), and are specified as follows [33, 36]: $K_C = 14.49\ k_\mathrm{B}T$, $\kappa_t = 9.5\ k_\mathrm{B}T\ \mathrm{nm}^{-2}$, $K_a = 28.93\ k_\mathrm{B}T\ \mathrm{nm}^{-2}$, $a_0 = 0.639\ \mathrm{nm}^2$, and $l_0 = 1.51$ nm. The spontaneous curvature of POPC is negligible [37], and therefore J_s is set to zero. Inserting these parameters into the highly-detailed model allows for the investigation of budding under experimentally and physiologically relevant conditions.

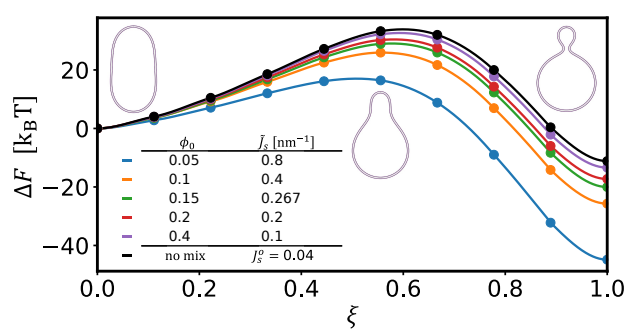

FIG. 4. The budding free energy pathway along the NEB reaction coordinate, ξ, for various vesicles with an average spontaneous curvature of 0.04 nm^{-1} in the outer leaflet, consistent with POPC vesicle parameters (see main text). Except for the non-mixing vesicle (black), the average spontaneous curvature arises from the additional lipid's intrinsic curvature, $\tilde{J}_s$, and its molar ratio, ϕ_0. The vesicle transitions from a prolate shape (left) to a pear shape (middle) and ultimately forms a neck, separating into distinct MV and DV (right); these images represent the minimized path of the non-mixing system.

The effect of lipid mixing on the budding free energy pathway is studied here, following experimental conditions involving outer leaflet lipid insertion [11, 17]. In this setup, 10% extra lipid volume is added to the outer

leaflet of an initially unstressed, symmetric POPC vesicle with a radius of 50 nm and 96% relative water content volume, as vesicles usually contain less water than ideal [3, 19]. Furthermore, the outer leaflet is set as an ideal binary mixture ($\chi = 0$) with an average spontaneous curvature $\phi_0 \cdot \tilde{J}_s$ of 0.04 nm^{-1}, which arises due to the presence of the additional lipid. The minimal free energy path for the budding of this vesicle is evaluated using the Nudged Elastic Band (NEB) method along a spatially defined reaction coordinate, ξ, ranging from a prolate ($\xi = 0$) to a budded state ($\xi = 1$); further details in Section S5. The trajectory was computed for different values of ϕ_0 (Fig. 4). An example path, as found for $\phi_0 = 0.1$, is shown in Movie S1.

Overall, lipid mixing reduces the free energy difference both for the barrier and the final state. This is consistent with its characteristic effect of destabilizing membrane structure [38, 39]. While lipid demixing, where lipids sort according to their curvature preference, leads to a slight increase in f^{mix}, it allows for a more substantial decrease in f^{el} throughout budding (Fig. S8). The main energy components that change during this process are bending, which increases, and area stretching, which decreases (Fig. S9). The energy barrier decreases from 33.9 $k_{\mathrm{B}}T$ for the non-mixed vesicle to 25.9 $k_{\mathrm{B}}T$ for $\tilde{J}_s = 0.4$ nm^{-1} and $\phi_0 = 0.1$. This reduction is driven by lipid mixing and could roughly double in a symmetric vesicle. The energy barrier drop should increase the transition rate by several orders of magnitude. Notably, these energy barriers are close to those suggested for membrane fusion [25, 27]. Therefore, when fusion occurs at the neck, the budding kinetics may determine its rate. This might be particularly relevant to biological processes, which typically involve asymmetric and heterogeneous membranes [4–6].

Lipid mixing can be incorporated into the original ADE model by adjusting the elastic parameters and area asymmetry, softening the membrane while increasing spontaneous curvature and asymmetry [22]. A similar adjustment scheme, derived in Section S6, applies to the current model. For instance, a non-mixing vesicle with $J_s^o \neq 0$ (similar to the black line in Fig. 4) is equivalent to a mixed one with $\tilde{J}_s = 0.4\,\mathrm{nm}^{-1}$ and $\phi_0 = 0.1$, after the following changes: K_C and K_a decrease to 13.62 $k_{\mathrm{B}}T$ and 28.77 $k_{\mathrm{B}}T$ nm^{-2}, with a 0.6% increase in area asymmetry and setting $J_s^o = 0.0425\,\mathrm{nm}^{-1}$. These parameters yield a budding path with a 26.0 $k_{\mathrm{B}}T$ energy barrier, closely matching the 25.9 $k_{\mathrm{B}}T$ for the mixed vesicle. Notably, including the tilt degree of freedom in the model has little effect on the energy barrier. Inhibiting tilt by increasing κ_t to 200 $k_{\mathrm{B}}T\,\mathrm{nm}^{-2}$ for the original non-mixing vesicle raised the barrier by only 0.6 $k_{\mathrm{B}}T$.

For non-ideal mixtures (Fig. S10), increasing the interaction parameter, χ, promoted budding to a certain extent. Specifically, increasing it from 0 to 2 further decreased the energy barrier for $\tilde{J}_s = 0.4$ nm^{-1} by 5.4 $k_{\mathrm{B}}T$ to 20.5 $k_{\mathrm{B}}T$. Nevertheless, the process is extremely sensitive to the relative water content and the degree of area asymmetry (Figs. S11, S12), so even a small change in these factors may induce or inhibit it. This possibly explains the reason for the experimental limitations in terms of accuracy, due to variations in vesicle properties within a sample or between fabrication methods.

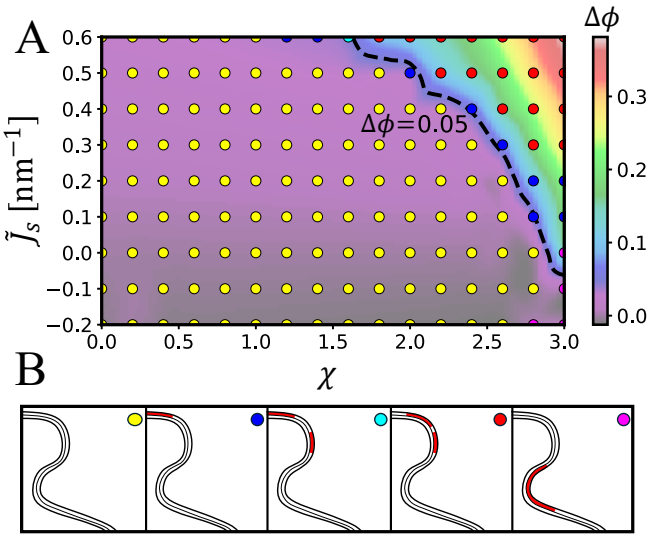

FIG. 5. (A) The influence of the additional lipid's spontaneous curvature, $\tilde{J}_s$, and the interaction parameter between the two lipids, χ, on compositional discrepancies between the DV and MV, $\Delta\phi$, and domain types (schematically illustrated in panel B) in equilibrium structures. Some setups form no domain (B, yellow), while others form a single domain at the top of the DV (B, blue), sometimes with an additional ring domain (B, cyan). Other scenarios include two ring domains (B, red) or a single domain at the neck (B, magenta). $\Delta\phi$ values were interpolated using a cubic spline and were less than 0.05 (dashed line) unless a domain formed.

Fig. 5A illustrates the compositional discrepancies between the DV and MV, $\Delta\phi = \langle\phi\rangle_{\mathrm{DV}} - \langle\phi\rangle_{\mathrm{MV}}$, as well as the formation of domains, which arise due to increases in $\tilde{J}_s$ and χ; details in Section S8. The model parameters are as previously described, except for an initial relative water content of 90% and setting $\phi_0 = 1/11 \approx 0.0909$ at the outer leaflet. Setting $\phi_0 = 0.2$ results in behavior similar to that detailed below (Fig. S7), provided that the average spontaneous curvature, $\phi_0 \cdot \tilde{J}_s$, covers a similar range of values. When parameter values are low, no domain forms. However, if χ is sufficiently high, a circular domain forms at the top of the DV ($\tilde{J}_s > 0$) or a ring domain forms at the neck ($\tilde{J}_s \leq 0$). Further increases in the two parameters lead to the formation of a ring domain around the circular one, which eventually also becomes a ring domain. Examples of these equilibrium structures are shown in Figs. S13-S16. We expect a richer phase diagram for real vesicles, as the model only addresses cylindrically symmetric structures [40].

With $\tilde{J}_s \geq 0.3$ nm^{-1}, multiple ring domains appear. In this case, the additional lipid's spontaneous curvature is larger than some micelle-forming surfactants [41]. There-

fore, it is unlikely that these ring domains which contain more than 90% of a micelle-forming lipid will be stable in real vesicles but instead will separate from them as mixed micelles—a process which is not accounted for by the current model.

Generally, $\Delta\phi$ is less than 0.05 (or 0.065 for $\phi_0 = 0.2$) unless a domain forms on the DV. Consequently, f^{mix} and, by extension, the mixing entropy for sufficiently low χ, dominates over f^{el} in its impact on the local composition. This agrees with other theoretical and experimental studies [31, 32, 42], where only a *relative* enrichment of less than 50% in some lipid component without phase separation in curved regions was observed. Notably, a recent experiment [17] under conditions similar to those modeled here reported up to a five-fold enrichment in lysolipid ($\tilde{J}_s \approx 0.2 - 0.4\ \mathrm{nm}^{-1}$) content in the DV. According to the model, such high enrichment should involve domain formation, which is unlikely in this case due to domain instability, as discussed above. This is also supported by MD simulations, which show that lysolipids in POPC should have $\chi \approx 0.6 \ll 2$ (Table S1), indicating a low tendency to phase separate.

In summary, the budding process in nanoscale vesicles was explored in a quantitative and controlled manner. The findings show that budding in such vesicles requires larger asymmetries. Additionally, careful modulation of membrane heterogeneity, area asymmetry, and osmotic conditions may allow for the regulation of budding dynamics. Finally, the composition of the DV is not substantially different from its MV unless phase separation occurs at the bud.

I. ACKNOWLEDGMENTS

I thank D. Harries, P. Jungwirth, M. Javanainen, B. Fabian and M. I. Morandi for meaningful discussions and their insightful comments. I thank ChatGPT for aiding with refining the manuscript. I acknowledge the European Regional Development Fund OP RDE (project ChemBioDrug no. CZ.02.1.01/0.0/0.0/16_019/0000729) and the ERC Advanced Grant no. 101095957. by the European Research Council for support and computational resources.

[1] M. Dubois-Dalcq, K. V. Holmes, and B. Rentier, *Assembly of Enveloped RNA Viruses* (Springer Science & Business Media, 2012).

[2] K. Denzer, M. J. Kleijmeer, H. F. Heijnen, W. Stoorvogel, and H. J. Geuze, Exosome: from internal vesicle of the multivesicular body to intercellular signaling device, J. Cell Sci. **113**, 3365 (2000).

[3] R. Lipowsky, Multispherical shapes of vesicles highlight the curvature elasticity of biomembranes, Adv. Colloid Interface Sci. **301**, 102613 (2022).

[4] M. S. Bretscher, Asymmetrical lipid bilayer structure for biological membranes, Nature New Biol. **236**, 11 (1972).

[5] A. Verkleij, R. Zwaal, B. Roelofsen, P. Comfurius, D. Kastelijn, and L. Van Deenen, The asymmetric distribution of phospholipids in the human red cell membrane. a combined study using phospholipases and freeze-etch electron microscopy, Biochim. Biophys. Acta. **323**, 178 (1973).

[6] G. Van Meer, D. R. Voelker, and G. W. Feigenson, Membrane lipids: where they are and how they behave, Nat. Rev. Mol. Cell Biol. **9**, 112 (2008).

[7] J. Lorent, K. R. Levental, L. Ganesan, G. Rivera-Longsworth, E. Sezgin, M. Doktorova, E. Lyman, and I. Levental, Plasma membranes are asymmetric in lipid unsaturation, packing and protein shape, Nat. Chem. Biol. **16**, 644 (2020).

[8] M. Takeda, K. Yamagami, and K. Tanaka, Role of phosphatidylserine in phospholipid flippase-mediated vesicle transport in saccharomyces cerevisiae, Eukaryot. Cell. **13**, 363 (2014).

[9] G. Heimlich, C. D. Bortner, and J. A. Cidlowski, Apoptosis and cell volume regulation: the importance of ions and ion channels, in *Cell Volume and Signaling* (Springer, 2005) pp. 189–203.

[10] L. Miao, U. Seifert, M. Wortis, and H.-G. Döbereiner, Budding transitions of fluid-bilayer vesicles: The effect of area-difference elasticity, Phys. Rev. E **49**, 5389 (1994).

[11] M. Krompers and H. Heerklotz, A guide to your desired lipid-asymmetric vesicles, Membranes **13**, 267 (2023).

[12] G. Pabst and S. Keller, Exploring membrane asymmetry and its effects on membrane proteins, Trends Biochem. Sci. **49**, 333 (2024).

[13] H.-T. Cheng, Megha, and E. London, Preparation and properties of asymmetric vesicles that mimic cell membranes, J. Biol. Chem. **284**, 6079 (2009).

[14] H.-T. Cheng and E. London, Preparation and properties of asymmetric large unilamellar vesicles: interleaflet coupling in asymmetric vesicles is dependent on temperature but not curvature, Biophys. J. **100**, 2671 (2011).

[15] R. A. Petazzi, A. Gramatica, A. Herrmann, and S. Chiantia, Time-controlled phagocytosis of asymmetric liposomes: Application to phosphatidylserine immunoliposomes binding hiv-1 virus-like particles, Nanomedicine **11**, 1985 (2015).

[16] B. Eicher, D. Marquardt, F. A. Heberle, I. Letofsky-Papst, G. N. Rechberger, M.-S. Appavou, J. Katsaras, and G. Pabst, Intrinsic curvature-mediated transbilayer coupling in asymmetric lipid vesicles, Biophys. J. **114**, 146 (2018).

[17] L. Hua, M. Kaiser, I. Carabadjac, A. Meister, G. Hause, and H. Heerklotz, Vesicle budding caused by lysolipid-induced asymmetry stress, Biophys. J. **122**, 4011 (2023).

[18] S. Karmakar, Particle size distribution and zeta potential based on dynamic light scattering: Techniques to characterize stability and surface charge distribution of charged colloids, Recent Trends Mater. Phys. Chem **28**, 117 (2019).

[19] B. Mui, P. Cullis, E. Evans, and T. Madden, Osmotic properties of large unilamellar vesicles prepared by extrusion, Biophys. J. **64**, 443 (1993).

[20] G. Jacquemet, A. F. Carisey, H. Hamidi, R. Henriques, and C. Leterrier, The cell biologist's guide to super-resolution microscopy, J. Cell Sci. **133**, jcs240713 (2020).

[21] C. Gupta, D. Sarkar, D. P. Tieleman, and A. Singharoy, The ugly, bad, and good stories of large-scale biomolecular simulations, Curr. Opin. Struct. Biol. **73**, 102338 (2022).

[22] U. Seifert, Curvature-induced lateral phase segregation in two-component vesicles, Phys. Rev. Lett. **70**, 1335 (1993).

[23] W. Helfrich, Elastic properties of lipid bilayers: theory and possible experiments, Z. Naturforsch. C. **28**, 693 (1973).

[24] M. Hamm and M. M. Kozlov, Elastic energy of tilt and bending of fluid membranes, Eur. Phys. J. E. **3**, 323 (2000).

[25] Y. Kozlovsky and M. M. Kozlov, Stalk model of membrane fusion: solution of energy crisis, Biophys. J. **82**, 882 (2002).

[26] R. J. Ryham, M. A. Ward, and F. S. Cohen, Teardrop shapes minimize bending energy of fusion pores connecting planar bilayers, Phys. Rev. E **88**, 062701 (2013).

[27] R. J. Ryham, T. S. Klotz, L. Yao, and F. S. Cohen, Calculating transition energy barriers and characterizing activation states for steps of fusion, Biophys. J. **110**, 1110 (2016).

[28] R. J. Ryham, Local changes in lipid composition to match membrane curvature, Comput. Math. Biophys. **4**, (2016).

[29] W. C. Wimley and T. Thompson, Exchange and flip-flop of dimyristoyl phosphatidylcholine in liquid-crystalline, gel and two-component, two-phase large unilamellar vesicles, Biochemistry **29**, 1296 (1990).

[30] S. Safran, *Statistical Thermodynamics of Surfaces, Interfaces, and Membranes* (CRC Press, 2018).

[31] B. Sorre, A. Callan-Jones, J.-B. Manneville, P. Nassoy, J.-F. Joanny, J. Prost, B. Goud, and P. Bassereau, Curvature-driven lipid sorting needs proximity to a demixing point and is aided by proteins, Proc. Natl. Acad. Sci. USA. **106**, 5622 (2009).

[32] G. Khelashvili, D. Harries, and H. Weinstein, Modeling membrane deformations and lipid demixing upon protein-membrane interaction: the bar dimer adsorption, Biophys. J. **97**, 1626 (2009).

[33] I. Schachter and D. Harries, Capturing lipid nanodisc shape and properties using a continuum elastic theory, J. Chem. Theory Comput. **19**, 1360 (2023).

[34] J. Jouhet, Importance of the hexagonal lipid phase in biological membrane organization, Front. Plant Sci. **4**, 494 (2013).

[35] S. M. Gruner, Intrinsic curvature hypothesis for biomembrane lipid composition: a role for nonbilayer lipids, Proc. Natl. Acad. Sci. USA. **82**, 3665 (1985).

[36] I. Schachter, C. Allolio, G. Khelashvili, and D. Harries, Confinement in nanodiscs anisotropically modifies lipid bilayer elastic properties, J. Phys. Chem. B. **124**, 7166 (2020).

[37] B. Kollmitzer, P. Heftberger, M. Rappolt, and G. Pabst, Monolayer spontaneous curvature of raft-forming membrane lipids, Soft Matter **9**, 10877 (2013).

[38] S. Leibler, Curvature instability in membranes, J. Phys. (Paris) **47**, 507 (1986).

[39] C.-M. Chen, P. Higgs, and F. MacKintosh, Theory of fission for two-component lipid vesicles, Phys. Rev. Lett. **79**, 1579 (1997).

[40] G. Golani, N. Ariotti, R. G. Parton, and M. M. Kozlov, Membrane curvature and tension control the formation and collapse of caveolar superstructures, Dev. Cell. **48**, 523 (2019).

[41] N. Fuller and R. Rand, The influence of lysolipids on the spontaneous curvature and bending elasticity of phospholipid membranes, Biophys. J. **81**, 243 (2001).

[42] E. A. Cino and D. P. Tieleman, Curvature-based sorting of eight lipid types in asymmetric buckled plasma membrane models, Biophys. J. **121**, 2060 (2022).